iScience

CellPress
OPEN ACCESS

Article

The role of osteocrin in memory formation during early learning, as revealed by visual imprinting in chicks

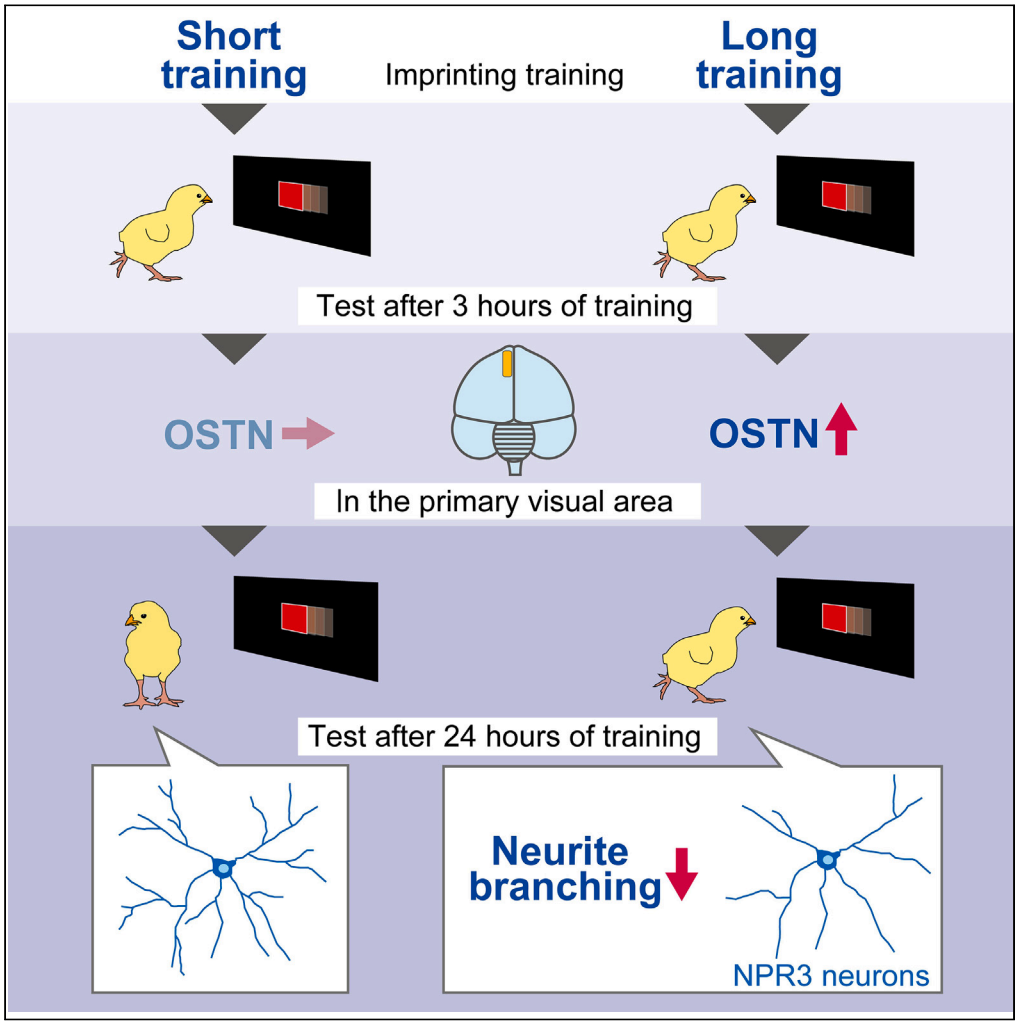

Tomoharu Nakamori, Izumi Komatsuzawa, Umi Iwata, ..., Tetsuya Kitaguchi, Takashi Tsuboi, Hiroko Ohki-Hamazaki

tom-naka@kitasato-u.ac.jp (T.N.)
hamazaki@kitasato-u.ac.jp (H.O.-H.)

Highlights

OSTN binds to NPR3 and reduces intracellular cAMP

OSTN and NPR3 are expressed in the primary visual area of the chick brain

Imprinting training increases OSTN levels, which improves memory retention

OSTN reduces neurite branching in the primary visual area

Nakamori et al., iScience 27, 111195
November 15, 2024 © 2024 The Author(s). Published by Elsevier Inc.
https://doi.org/10.1016/j.isci.2024.111195

iScience

CellPress
OPEN ACCESS

Article

The role of osteocrin in memory formation during early learning, as revealed by visual imprinting in chicks

Tomoharu Nakamori,[1,6,*] Izumi Komatsuzawa,[1] Umi Iwata,[1] Ami Makita,[1] Go Kagiya,[2] Kazuko Fujitani,[3] Tetsuya Kitaguchi,[4] Takashi Tsuboi,[5] and Hiroko Ohki-Hamazaki[1,*]

SUMMARY

Osteocrin (OSTN) is structurally associated with natriuretic peptides. Its expression in the brain, which has only been recognized in anthropoid primates, is induced by sensory stimuli and regulates the activity-dependent dendritic growth of neurons. However, details on the signaling mechanisms of OSTN and its function in plastic changes during learning and memory have yet to be elucidated. We found that OSTN was expressed in the cortical region of the chicken brain. The injection of chicken OSTN (chOSTN) after imprinting training prolonged the memory retention for the imprinting stimulus. Conversely, a reduction in the OSTN receptor chNPR3 inhibited memory retention. The memory retention was positively correlated with a high level of chOSTN and fewer neurites in the cortical region. In conclusion, OSTN-NPR3 signaling promoted memory consolidation and/or retention by regulating neurite branching during childhood.

INTRODUCTION

The construction and reorganization of neural circuits in the central nervous system (CNS) during early childhood is essential for the development of brain function. Newly hatched precocial bird chicks quickly learn the characteristics of their mothers and follow them. This learning behavior called imprinting,[1] which can be elicited by an object to which they are exposed, occurs only in the short period after hatching, and robust memory is maintained for a long time. We have previously demonstrated that the neural pathway in the telencephalon is crucial for visual imprinting in chicks.[2] This pathway connects two regions that are important for imprinting behavior: the visual Wulst (VW) and the intermediate medial mesopallium (IMM), which correspond to the mammalian visual and association cortices, respectively. The establishment of visual imprinting increases the activity of neurons in the ventral region of the VW in response to visual stimuli[3] while suppressing the activity of cells in the dorsal region of the VW,[4] resulting in restricted neural activity within the neural pathway.[5,6] However, the known effect of imprinting on neural morphology is that training has a positive effect on the dendritic spine volume in the apical hyperpallium (HA) and the length of postsynaptic density of spine synapses in the left IMM.[7,8] The elucidation of the molecular mechanism underlying the change in neural activity requires additional analysis of the structural changes in the neural circuit.

We previously demonstrated that high expression of C-type natriuretic peptide 3 (CNP3) was observed in the VW region of chicks during the critical period of imprinting behavior[9] and that CNP3 was thought to be involved in the establishment of imprinting. In addition, we detected osteocrin (OSTN) expression in the VW of posthatching chicks.

OSTN, also known as musclin, is a small, secreted protein. In mammals, OSTN mRNA is mainly expressed in osteoblasts and skeletal muscles.[10,11] The precursor OSTN protein is thought to be cleaved at two sites (KKKR and KRR) and the resulting mature OSTN peptides show partial homology with natriuretic peptides (NPs).[12] In mice, three receptors (NPRs) with an affinity for NP are known: NPR1, NPR2, and NPR3. Mouse OSTN binds selectively to NPR3 but not to NPR1 or NPR2.[12,13] Both NPR1 and NPR2 contain a guanylyl cyclase (GC) domain that synthesizes cyclic guanosine monophosphate (cGMP) when stimulated with NP.[14–17] NPR3, which has a short intracellular region lacking the GC domain, is considered to act only as a clearance receptor without a signal-transducing function.[18,19] Indeed, transgenic mice overexpressing OSTN have elongated bones and elevated cGMP levels, suggesting that OSTN modulates the actions of CNP3 in the bone by inhibiting the clearance activity of NPR3 by CNP3.[12,20] However, evidence indicates that NPR3 is coupled to a pertussis toxin-sensitive inhibitory G protein (Gi) and reduces adenylyl cyclase activity and intracellular cyclic adenosine monophosphate (cAMP) levels,[21–23] suggesting the existence of signal transduction elicited by OSTN via NPR3.

[1]College of Liberal Arts and Sciences, Kitasato University, Kitasato, Minami-ku, Sagamihara, Kanagawa 252-0373, Japan
[2]School of Allied Health Sciences, and Regenerative Medicine and Cell Design Research Facility, Kitasato University, Kitasato, Minami-ku, Sagamihara, Kanagawa 252-0374, Japan
[3]Gene Analysis Center, School of Medicine, Kitasato University, Kitasato, Minami-ku, Sagamihara, Kanagawa 252-0374, Japan
[4]Laboratory for Chemistry and Life Science, Institute of Innovative Research, Tokyo Institute of Technology, Nagatsuta-cho, Midori-ku, Yokohama, Kanagawa 226-8503, Japan
[5]Department of Life Sciences, Graduate School of Arts and Sciences, The University of Tokyo, Komaba, Meguro-ku, Tokyo 153-8902, Japan
[6]Lead contact
*Correspondence: tom-naka@kitasato-u.ac.jp (T.N.), hamazaki@kitasato-u.ac.jp (H.O.-H.)
https://doi.org/10.1016/j.isci.2024.111195

This is an open access article under the CC BY-NC-ND license (http://creativecommons.org/licenses/by-nc-nd/4.0/).

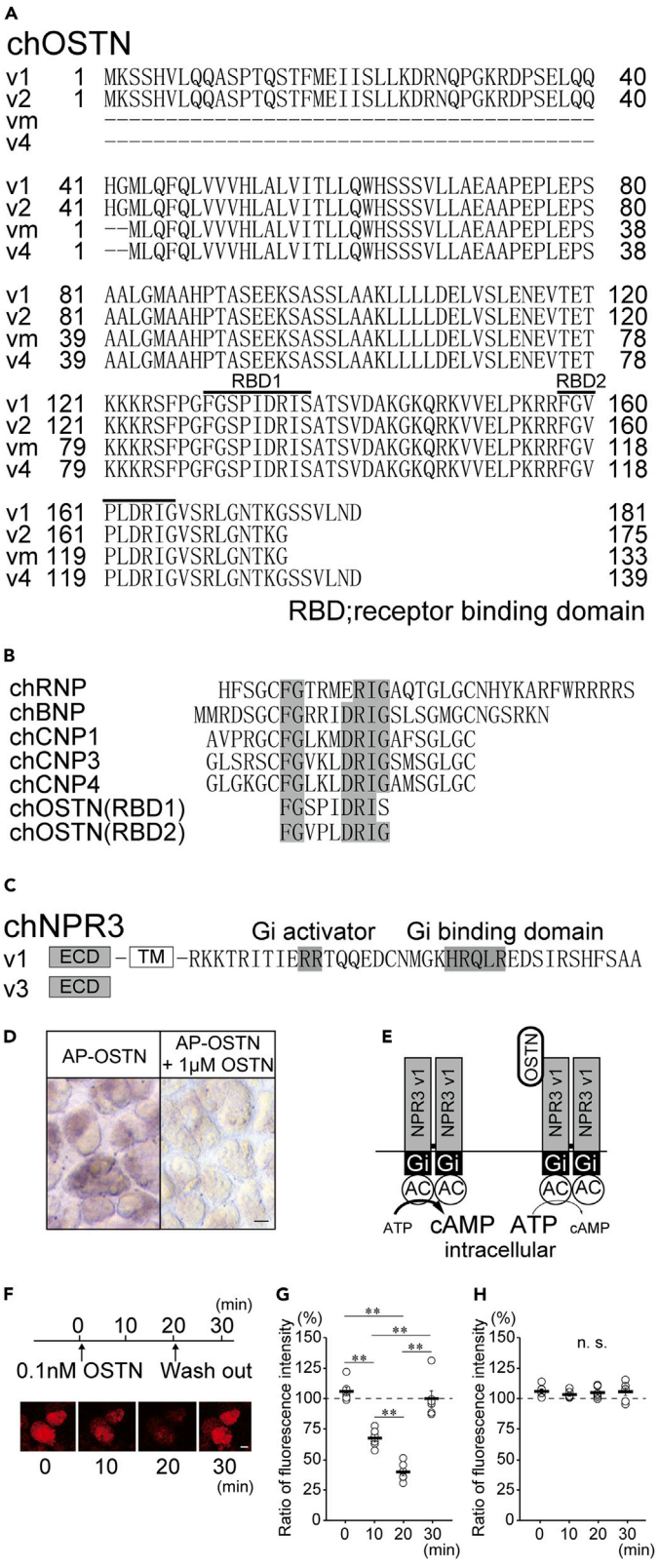
A
chOSTN
v1 1 MKSSHVLQQASPTQSTFMEIISLLKDRNQPGKRDPSELQQ 40
v2 1 MKSSHVLQQASPTQSTFMEIISLLKDRNQPGKRDPSELQQ 40
vm ----------
v4 ----------
v1 41 HGMLQFQLVVVHLALVITLLQWHSSSVLLAEAAPEPLEPS 80
v2 41 HGMLQFQLVVVHLALVITLLQWHSSSVLLAEAAPEPLEPS 80
vm 1 --MLQFQLVVVHLALVITLLQWHSSSVLLAEAAPEPLEPS 38
v4 1 --MLQFQLVVVHLALVITLLQWHSSSVLLAEAAPEPLEPS 38
v1 81 AALGMAAHPTASEEKSASSLAAKLLLLDELVSLENEVTET 120
v2 81 AALGMAAHPTASEEKSASSLAAKLLLLDELVSLENEVTET 120
vm 39 AALGMAAHPTASEEKSASSLAAKLLLLDELVSLENEVTET 78
v4 39 AALGMAAHPTASEEKSASSLAAKLLLLDELVSLENEVTET 78
RBD1
RBD2
v1 121 KKKRSFPGFGSPIDRISATSVDAKGKQRKVVELPKRRFGV 160
v2 121 KKKRSFPGFGSPIDRISATSVDAKGKQRKVVELPKRRFGV 160
vm 79 KKKRSFPGFGSPIDRISATSVDAKGKQRKVVELPKRRFGV 118
v4 79 KKKRSFPGFGSPIDRISATSVDAKGKQRKVVELPKRRFGV 118
v1 161 PLDRIGVSRLGNTKGSSVLND 181
v2 161 PLDRIGVSRLGNTKG 175
vm 119 PLDRIGVSRLGNTKG 133
v4 119 PLDRIGVSRLGNTKGSSVLND 139
RBD;receptor binding domain
B
chRNP HFSGCFGTRMERIGAQTGLGCNHYKARFWRRRRS
chBNP MMRDSGCFGRRIDRIGSLSGMGCNGSRKN
chCNP1 AVPRGCFGLKMDRIGAFSGLGC
chCNP3 GLSRSCFGVKLDRIGSMSGLGC
chCNP4 GLGKGCFGLKLDRIGAMSGLGC
chOSTN(RBD1) FGSPIDRIS
chOSTN(RBD2) FGVPLDRIG
C
chNPR3
Gi activator
Gi binding domain
v1 ECD – TM –RKKTRITIERRTQQEDCNMGKHRQLREDSIRSHFSAA
v3 ECD
D
AP-OSTN
AP-OSTN + 1μM OSTN
E
OSTN
NPR3 v1
NPR3 v1
NPR3 v1
NPR3 v1
Gi
Gi
Gi
Gi
AC
AC
AC
AC
ATP
cAMP
ATP
cAMP
intracellular
F
(min)
0 10 20 30
0.1nM OSTN
Wash out
0 10 20 30
(min)
G
Ratio of fluorescence intensity
(%)
150
125
100
75
50
25
0
**
0 10 20 30
(min)
H
Ratio of fluorescence intensity
(%)
150
125
100
75
50
25
0
n. s.
0 10 20 30
(min)

Figure 1. Structure of chOSTN and NPR3, and the ability of OSTN to mediate signaling through the reduction of cAMP production in NPR3-expressing cells

(A) The amino acid sequences of chOSTN peptide. Two predicted receptor-binding domains (RBDs) are present in chOSTN.

(B) Comparison of the amino acid sequences of mature chicken NP and the partial sequences of chOSTN containing RBD. Amino acid residues that are conserved among chicken NP are marked with gray filling.

(C) Structures of chNPR3v1 and v3 transcripts, and the amino acid sequence of the intracellular domain. ChNPR3v1 contains an intracellular Gi activator and a Gi-binding domain, whereas chNPR3v3 has no transmembrane domain (TM). ECD, extracellular domain.

(D) AP-OSTN binding to NPR3v1-expressing cells (left) and its inhibition by the addition of 1 μM OSTN (right). Scale bar, 10 μm.

(E) Schematic representation of the extracellular and intracellular domains of chNPR3v1. When OSTN binds to chNPR3v1, a decrease in intracellular cAMP production is expected.

(F) Experimental schedules and sequential images of chNPR3v1 cells expressing Pink Flamindo after exposure to 0.1 nM OSTN. Scale bar, 10 μm.

(G) Time course of fluorescence intensity of chNPR3v1 cells expressing Pink Flamindo (n = 120 cells from six experiments). The addition of OSTN reduced the fluorescence intensity.

(H) Time course of fluorescence intensity of HEK293 cells expressing Pink Flamindo (n = 120 cells from six experiments). No change in fluorescence intensity was observed with the exposure to OSTN. Data are represented as mean ± SEM. **, $p < 0.01$; n.s., not significant. See also Figures S1 and S2, and Tables S1 and S2.

The expression and function of OSTN in the CNS has only been reported by Ataman et al.[24] They showed that in the primate neocortex, OSTN is expressed in glutamatergic neurons of layer 4C and restricts activity-dependent dendritic growth in cultured human fetal neurons, although it remains unclear which receptor is involved. The expression of OSTN in the brain has not yet been confirmed in species other than primates, which limits the functional analysis of OSTN in the CNS.

In this study, we demonstrated the function of OSTN in learning-induced neural plastic changes by exploiting its expression in chick VW, which is critical for visual imprinting. We showed that OSTN and the NPR3 were expressed in the telencephalon of chicks after hatching. Behavioral experiments and histological analyses revealed that OSTN-NPR3 signaling plays an important role in the restriction of neurite branching that occurs during the consolidation process of memory for the imprinting stimulus.

RESULTS

Structure of chicken OSTN and NPR3, and the ability of OSTN to mediate signaling through the reduction of cAMP production in NPR3-expressing cells

The chicken OSTN (chOSTN) gene is located on chromosome 9 and has at least four transcript variants: the major transcript variant (vm), GenBank: NM_001098608, variant 1 (v1), GenBank: XM_025153364, v2, GenBank: XM_025153365, and v4, GenBank: XM_015291403. Each transcript variant had two common domains, the receptor-binding domain (RBD), similar to OSTN in other species (Figure 1A).[12,13] The sequences in the N- and C-terminal regions differed between the transcript variants. The two RBDs had sequences highly similar to the predicted receptor-binding regions of chicken NP: chRNP (GenBank: NM_001198747), chBNP (GenBank: NM_204925), chCNP1 (GenBank: NM_001193616), chCNP3 (GenBank: NM_001111259), and chCNP4 (GenBank: XM_015291500) (Figure 1B).

In mammals, OSTN binds to NPR3.[12,13] The v1 gene transcript of chicken NPR3 (chNPR3, GenBank: XM_046936337) is similar to that of mammalian NPR3, which has a Gi activator sequence and a Gi-binding domain in the intracellular region[23,25] and is considered a Gi-binding receptor (Figure 1C).

To confirm the binding of chOSTN to the chNPR3, chOSTN fused with secreted alkaline phosphatase (AP-OSTN) or unfused AP protein (Figure S1) was prepared[12] and reacted with chNPR3v1-expressing HEK293 cells (chNPR3v1 cells, Figure S2). AP activity was detected exclusively in the chNPR3v1 cells that reacted with AP-OSTN. No AP activity was detected when the reaction was performed in the presence of the synthetic chOSTN peptide, indicating that the chOSTN peptide containing RBD2 bound to chNPR3 (Figure 1D). In mammals, NPR3 is considered to be a dimer with a Gi-binding domain in the intracellular region,[26] and ligand binding is thought to suppress the activity of adenylate cyclase and reduce cAMP production from ATP (Figure 1E).[21–23] To investigate whether chOSTN regulates intracellular cAMP levels via chNPR3v1 in living cells, we used chNPR3v1 cells expressing the red fluorescent protein-based cAMP indicator Pink Flamindo.[27] The cAMP levels were reduced by the addition of 0.1 nM chOSTN peptide and were then recovered to the initial levels after washing out the chOSTN (Figures 1F and 1G; Table S1). In HEK293 cells expressing Pink Flamindo, the addition of chOSTN did not affect the levels of cAMP (Figure 1H; Table S2).

Prominent expression of OSTN in the left HA and constant expression of NPR3 in the left dorsal telencephalon of posthatching chicks

The expression of chOSTN vm and v4 transcripts in the chick left rostral HA in the VW region, which is essential for visual imprinting,[2,5] and in the left dorsal telencephalon of the chick embryo, was examined using reverse-transcription PCR (RT-PCR) at E8, E12, E16, P1, and P7. The expression levels of the chOSTN vm and v4 transcripts were higher after hatching than at the embryonic stage (Figure 2A; Figure S3). In contrast, v1 and v2 gene transcripts were detected at E8 but not at P1 and P7 (data not shown). Next, we examined the expression of OSTN transcripts in the left telencephalon of P1 chicks using *in situ* hybridization. Cells expressing OSTN were localized in the HA in the VW and dorsal areas of the amygdala/arcopallium (Figures 2B and 2C; Figures S4 and S5). OSTN-expressing cells were observed in the lateral area of the nidopallial caudal island field (NCIF), superficial part of the ventral mesopallium (MVS), and superficial part of the dorsal

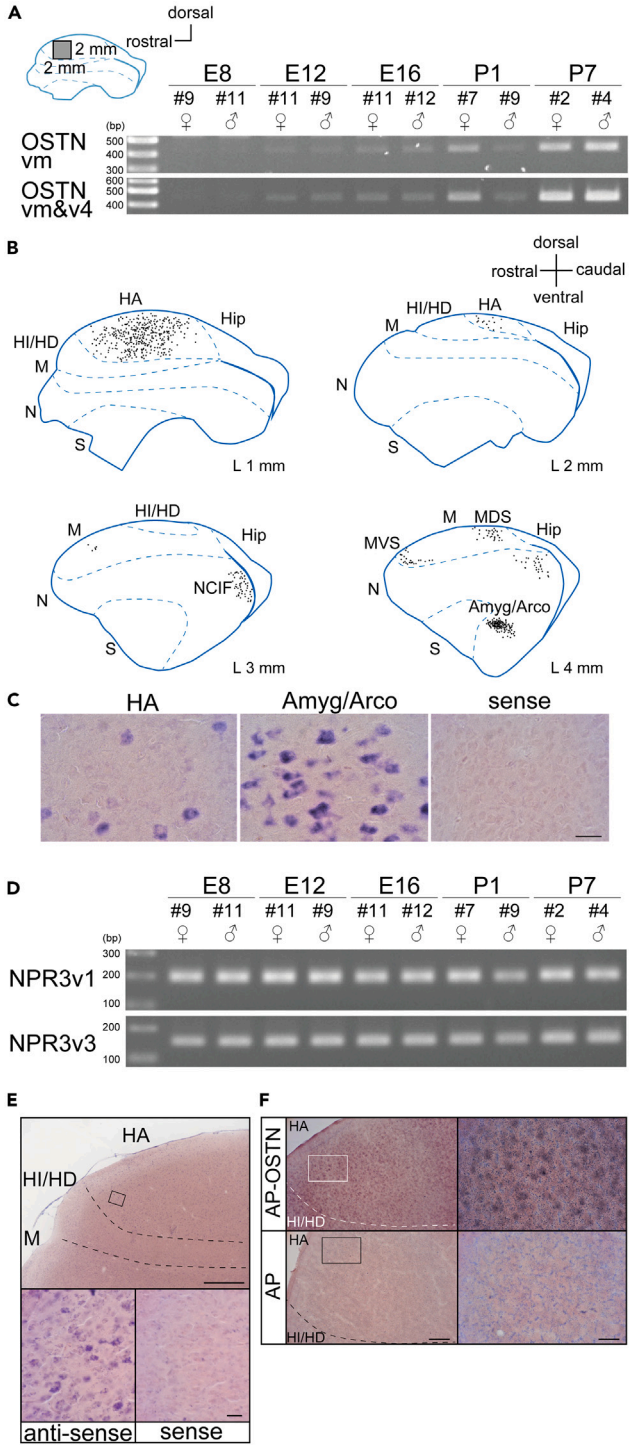

Figure 2. Prominent expression of OSTN in the HA and constant expression of NPR3 in the left dorsal telencephalon of posthatching chicks

(A) Schema showing the sampling area in the sagittal section (L 1 mm) of the left telencephalon. The expression of chOSTN transcripts in the brain (the dorsocaudal region of the left telencephalon at embryonic stages and the left rostral HA at posthatching stages as shown in the schema), as revealed by RT-PCR analysis. Control reactions using chGAPDH gene primers for each sample are presented in Figure S3.

(B) Schematic diagram of the distribution of cells expressing chOSTN mRNA in the P1 telencephalon (sagittal section). The number (mm) at the bottom right of each diagram shows the corresponding position (distance from the midline) indicated in the sagittal figures of the chick brain atlas.[28].

(C) Representative photographs of chOSTN mRNA expression in the HA (left) and Amyg/Arco (center), and an image of the section reacted with the sense probes (right). Scale bar, 20 μm. Amyg/Arco, amygdala/arcopallium; HA, hyperpallium apicale; HI/HD, the hyperpallium intercalatum and hyperpallium densocellulare

Figure 2. *Continued*

layer in the VW; Hip, hippocampus; L, lateral; M, mesopallium; MDS, superficial part of the dorsal mesopallium; MVS, superficial part of the ventral mesopallium; N, nidopallium; NCIF, the nidopallial caudal island field; S, subpallium.

(D) Expression of chNPR3 transcripts in the brain, as revealed by RT-PCR analysis. The samples used are the same as in Figure 2A.

(E) Representative photographs of NPR3 mRNA expression in the P1 VW (upper; scale bar, 500 μm). A high magnification image of mRNA expressed cells in the areas surrounded by lines (lower left), and an image of the section reacted with the sense probes (lower right; scale bar, 20 μm).

(F) AP staining of AP-OSTN or AP reacted with the brain slices of P1 chicks (left, scale bar, 200 μm), and enlarged images of the area surrounded by lines (right, scale bar, 20 μm). Positive staining is observed with AP-OSTN, not with AP. See also Figures S3–S5.

mesopallium (MDS). NCIF corresponds to the mammalian prefrontal cortex; MVS afferently projects to the IMM, while MDS also projects to the IMM.

In the left rostral HA of posthatching chicks, and in the left dorsal telencephalon of the chick embryos, NPR3v1 expression was confirmed as early as E8 and continued until P7 (Figure 2D). At P1, many NPR3 mRNA-positive cells were uniformly present in the HA where OSTN-expressing cells were observed (Figure 2E). Furthermore, when the distribution of cells that could bind OSTN was examined using AP-OSTN in frozen brain sections of P1 chicks, cells showing AP activity were observed in the HA, where the NPR3 mRNA was expressed (Figure 2F).

Expression of chOSTN increased 6 h after imprinting training, and chOSTN together with chNPR3 promoted consolidation of memory for the imprinting stimulus

The critical period during which the chicks could be visually imprinted was from P0 to P4 (Figure 3A).[2] When the development-dependent change in the posthatching period of OSTN expression in the left rostral HA was investigated by real-time PCR, we found that the expression level after the end of the critical period (P7, 0.27 ± 0.04, $n = 12$) was significantly higher than during the critical period (P1, 0.13 ± 0.02, $n = 12$; Figure 3B, t test, $p < 0.01$).

To investigate the effect of imprinting training on OSTN expression levels, the change in OSTN mRNA levels in the left rostral HA over time from the 30-min imprinting training at P1 was clarified. The expression level of OSTN significantly increased 6 h after the end of training (T(6h)), and this high expression level compared to the control was maintained even after 6 days (T(6d)). There was no difference in the expression levels of OSTN between the control and T(3h) or P2 chick without imprinting training (D(P2)) (Figure 3C; Table S3; $n = 12$ for each). Because the expression level of OSTN increased after training, OSTN was supposed to play a role after imprinting training was completed. Therefore, we investigated the function of the OSTN in consolidating acquired memory.

When 20 min of training (20m T) was performed instead of 30 min (30m T), the preference score (PS) for the imprinting stimulus was significantly higher than the chance level (PS = 0.5) at T(3h), although the PS was at the chance level at T(24h) (Figures 3D and 3E; T(3h), 0.67 ± 0.03, t test, $p < 0.01$; T(24h), 0.53 ± 0.01, t test, $p = 0.22$; $n = 12$ for each). When training was performed for 30 min (30m T), the chicks showed a significantly higher PS than the chance level at T(3h) and T(24h) (Figures 3D and 3E; T(3h), 0.71 ± 0.05, t test, $p < 0.01$; T(24h), 0.74 ± 0.04, t test, $p < 0.01$; $n = 12$ for each). A significant difference was observed between PS at T(3h) and T(24h) in the 20m T (paired t test, $p < 0.05$) but not in the 30m T (paired t test, $p = 0.21$). The expression levels of OSTN and NPR3 mRNA in the indicated area of the left rostral HA (Figure 3B inset) immediately after T(24h) were examined for each condition. OSTN mRNA expression in the 20m T was lower than that in the 30m T (Figure 3F; 20m T, 0.14 ± 0.01; T(24h), 0.24 ± 0.01; t test, $p < 0.05$, $n = 12$ for each). The expression level of NPR3 mRNA did not differ between the two groups (Figure 3G; 20m T, 0.43 ± 0.01; 30m T, 0.43 ± 0.01; t test, $p = 0.95$, $n = 12$ for each). The number of wheel rotations toward the screen per minute during training was higher in the 30m T than in the 20m T (Figure S6 left). This difference was due to a rapid increase in the number of wheel rotations 17 min after the start of training (Figure S6 right).

We then exploited weak training (20m T) to observe the facilitative effect of OSTN addition and standard training (30m T) to observe the inhibitory effect of NPR3 reduction. Three hours after 20m T, 2 μL of phosphate buffer (PB) containing 1 nM chOSTN peptide or PB was injected into the left HA region of chicks, and the PS was examined at T(24h). OSTN-injected group showed PS significantly higher than the chance level even at T(24h), but the group injected with PB did not (Figures 3H, 3I, and 3J; OSTN, 0.66 ± 0.04, t test, $p < 0.01$; PB, 0.55 ± 0.03, t test, $p = 0.17$; $n = 10$ for each).

To confirm the involvement of NPR3 in the process of memory consolidation, chicks in which the expression level of the NPR3 in the left HA was reduced were generated using short hairpin RNA interference (shRNAi). The efficiency of suppression by NPR3-RNAi vectors was evaluated in a chNPR3-expressing HEK293 cell line, and a reduction of approximately 83% was detected (Figure S7). We confirmed that when the control EGFP vectors (pEGFP-N2) were injected at ventral portion of the rostral HA and this brain area was subjected to *in vivo* electroporation, the EGFP-expressing cells were clustered in the targeted site in the ventral portion of the OSTN expression site in the rostral HA (Figure S8).

When shRNAi for NPR3 was performed 24 h before 30m T, these chicks (30m T-NPR3i) showed a significantly higher PS than the chance level at T(3h) but did not at T(24h) (Figures 3K and 3L; T(3h), 0.73 ± 0.05, t test, $p < 0.01$; T(24h), 0.54 ± 0.03, t test, $p = 0.41$; paired t test, $p < 0.01$; $n = 12$ for each). Chicks transfected with the scrambled shRNA vector (30m T-SCi) showed significantly higher PS than the chance level even at T(24h) (Figures 3K and 3L; T(3h), 0.71 ± 0.04, t test, $p < 0.01$; T(24h), 0.75 ± 0.03, t test, $p < 0.01$; paired t test, $p = 0.13$; $n = 12$ for each).

The expression levels of OSTN and the NPR3 mRNA in the indicated area of the left rostral HA (Figure 3B inset) immediately after T(24h) were examined for each condition. OSTN mRNA expression in the 30m T-NPR3i was comparable to the 30m T-SCi (Figure 3M; 30m T-NPR3i, 0.27 ± 0.01; 30 mT-SCi, 0.22 ± 0.01; t test, $p = 0.32$, $n = 12$ for each). In addition, the expression level of the NPR3 mRNA in the 30m T-NPR3i

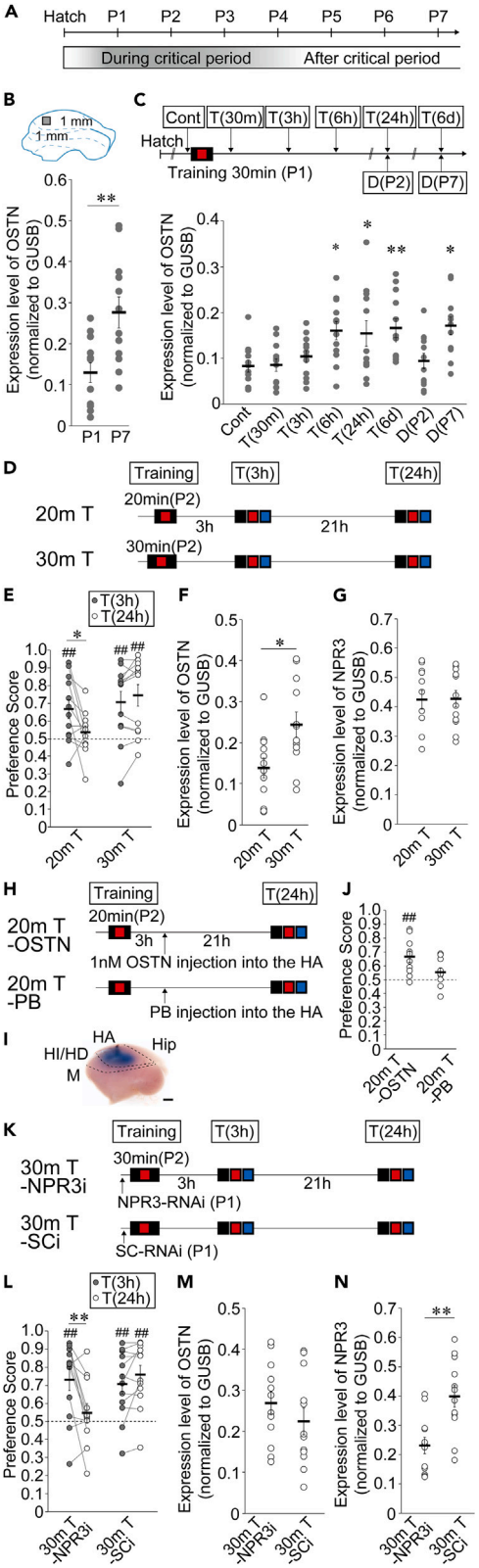

Figure 3. Expression of chOSTN increased 6 h after imprinting training, and chOSTN together with chNPR3 promoted consolidation of memory for the imprinting stimulus

(A) Visual imprinting in chicks only occurs during 4 days after hatching.

(B) Schema showing the sampling area in the sagittal section (L 1 mm) of the left telencephalon. Real-time PCR revealed that the expression level of OSTN mRNA in the rostral HA (indicated in the schema) was higher at P7 than at P1 in male chicks (n = 12 for each).

(C) Sampling schedule and comparison of the expression levels of OSTN mRNA (n = 12 for each). The expression level of OSTN significantly increased after 6 h of the training (T(6h)), and remained higher than control at 24 h (T(24h)) and 6 days (T(6d)) after training.

(D) Schedule for 20-min training (20m T) and 30-min training (30m T) and evaluations.

(E) Preference score at T(3h) and T(24h) of each group (n = 12 for each). At T(24h), only the 30m T chicks showed the score significantly higher than the chance level.

(F) The expression level of OSTN mRNA after T(24h) in the area indicated in Figure 3B inset was higher in the 30m T than 20m T chicks (n = 12 for each).

(G) The expression level of NPR3 mRNA after T(24h) in the area indicated in Figure 3B inset was comparable in the two groups. (n = 12 for each).

(H) Schedule of microinjection of OSTN or PB and behavioral experiments.

(I) Representative photograph showing a brain section from a chick injected with a solution containing 0.1% Evans blue dye in the HA; the injected site is recognized by blue staining. Scale bar, 1 mm.

(J) Preference score at T(24h) of each group (n = 10 for each). The preference score at T(24h) in the OSTN group was significantly higher than the chance level. Injection of OSTN into the HA significantly prolonged the retention time of memory.

(K) Schedule of inhibition of NPR3 expression using RNAi technique and behavioral experiments.

(L) Preference score at T(3h) and T(24h) of each group (n = 12 for each). The preference score at T(24h) in the NPR3i group was significantly lower than the chance level even after 30m T. Reducing NPR3 expression in the HA inhibited 24-h retention of memory.

(M) The expression level of OSTN mRNA after T(24h) in the area indicated in Figure 3B inset was comparable in the two groups (n = 12 for each).

(N) The expression level of NPR3 mRNA after T(24h) in the same area was lower in the NPR3i group than in SCi group (n = 12 for each). Data are represented as mean ± SEM. *, $p < 0.05$; **, ##, $p < 0.01$. See also Figures S6–S9 and Table S3.

was lower than the 30m T-SCi (Figure 3N; 30 mT-NPR3i, 0.23 ± 0.01; 30m T-SCi, 0.40 ± 0.02; t test, $p < 0.01$, $n = 12$ for each). The number of wheel rotations toward the screen per minute during training was comparable between the 30m T-NPR3i and the 30m T-SCi (Figure S9).

This showed that the knockdown of the chNPR3 gene in the left HA lowered the imprinting performance at T(24h), even when the level of OSTN transcripts was sufficiently high.

OSTN reduced the number of neurites in the embryonic brain, and long-term memory for the imprinting stimulus correlated with increased OSTN levels and reduced neurite branching in the left HA

OSTN is expressed in the primate neocortex and restricts the activity-dependent dendritic growth of human neurons.[24] Therefore, we investigated whether the memory-consolidating effect of OSTN is related to morphological changes in brain neurons caused by OSTN.

First, we used embryonic chick brain cultures because the inhibitory role of OSTN on neurite growth has only been demonstrated in human fetal brain neurons. In the E8 (13 days before hatching) chick brain, the NPR3 was already expressed, but OSTN was not (Figures 2A–2D). Using the E8 chick left brain, the effect of exogenous OSTN on neurite outgrowth was investigated in telencephalic slice culture. When neurons in the HA were labeled with EGFP by electroporating pEGFP-N2 vectors, and the number of neurites crossing concentric circles from the center of the cell body was measured, the number of neurites significantly decreased in the presence of 1 nM OSTN (Figures 4A and 4B; Table S4). More detailed analysis revealed that although the effect of OSTN on neither the number and mean length of the main shaft (neurites germinating from the nerve cell body) nor the mean neurite branch length was significant (Figure 4C; number of main shafts, 0 nM OSTN, 13.1 ± 1.5, 1 nM OSTN, 10.1 ± 0.87, t test, $p = 0.09$; length of main shafts [μm], 0 nM OSTN, 23.2 ± 3.2, 1 nM OSTN, 25.7 ± 2.2, t test, $p = 0.52$; length of neurite branch [μm], 0 nM OSTN, 7.3 ± 0.70, 1 nM OSTN, 8.6 ± 0.61, t test, $p = 0.18$), the number of neurite branch was significantly reduced by the addition of OSTN (Figure 4C; 0 nM OSTN, 31.6 ± 5.0, 1 nM OSTN, 17.5 ± 2.6, t test, $p < 0.05$). Moreover, when NPR3 expression was suppressed by shRNAi in the presence of OSTN, the number of neurites in chick embryonic brain cells significantly increased (Figures 4D and 4E; Table S5). These results show that OSTN, in combination with NPR3, inhibited the increase in the number of neurites during the embryonic period.

Next, we performed Golgi staining of HA neurons in P3 chicks to investigate whether changes in the number of neurites generated by OSTN-NPR3 signaling were involved in the process of memory consolidation that occurs after hatching.

First, the effects of the training time or expression level of NPR3 on the number of neurites were studied. At 24 h after training (T(24h)), the number of neurites in HA neurons was higher in the 20m T than in the 30m T (Figures 4F and 4G; Table S6). Suppression of NPR3 expression with shRNAi before 30-min training rescued the reduction in the number of neurites in HA neurons 24 h after training (Figure 4H; Table S7).

Then, taking advantage of the individual differences in imprinting performance, chicks showing high PS (PS > 0.70) at T(3h) and T(24h) were designated as good learners (PS = 0.87 ± 0.03 at T(3h) and 0.88 ± 0.02 at T(24h), $n = 8$), and chicks showing high PS (PS > 0.70) at T(3h), but low PS (PS < 0.60) at T(24h) (PS = 0.83 ± 0.03 at T(3h) and 0.53 ± 0.01 at T(24h), $n = 8$) were designated as poor learners (Figures 4I and 4J; T(3h), t test, $p = 0.38$; T(24h), t test, $p < 0.01$). The number of wheel rotations toward the screen per minute during training was higher for the good learners than for the poor learners (Figures S10 and S11).

The brains were removed immediately after T(24h), and we investigated whether learning performance was related to brain OSTN levels as well as the number of neurites in HA neurons. When the OSTN concentration in the indicated area of the left rostral HA (Figure 3B inset) was quantified, it was higher in the brain of the good learners than that of the poor learners (Figure 4K; good learners, 5.9 ± 0.92 pg/mg tissue; poor learners, 3.6 ± 0.32 pg/mg tissue; t test, $p < 0.05$). We performed Golgi staining using eight brains from each group and compared the number of neuronal protrusions in the left HA of good and poor learners. The number of neurites per neuron in the HA was significantly lower in the good learners than in the poor learners (Figure 4L; Table S8).

DISCUSSION

In the present study, we clarified the function of OSTN in early learning. In chicks, OSTN-expressing cells localized in the rostral HA, a telencephalic region indispensable for imprinting behavior, acted critically on the retention of memory for the imprinting stimulus via the activation of the NPR3. In addition, it was suggested that the reduction in neurite branching mediated by OSTN-NPR3 signaling in the left HA plays a pivotal role in memory retention. Visual imprinting affects the area of the left VW activated by a specific stimulus[5] and modifies neuronal activity in the left VW, resulting in the allocation of different cells to respond to imprinting or novel stimulus.[4] The inhibition of neurite branching by OSTN may prevent the formation of new connections and promote the fixation of preexisting connections between neurons, thus completing the neural pathway crucial for responding to the imprinting stimulus.

In this study, we did not attempt to distinguish between the effects of memory for the imprinting stimulus and predisposed preference. However, because the untrained chicks do not show a following response to the red square image on the monitor,[3] and for the reasons explained further, our behavioral experiment focused on memory for the imprinting stimulus rather than on predisposed preference. First, we observed an increased number of rotations per minute toward the screen during training in the 30m T group compared to the 20m T group, due to a rapid increase in the following response with time. This indicated that the following response was stronger in the 30m T than in the 20m T (Figure S6). Second, the following responses during the training were stronger in the good learners than in the poor learners (Figure S10). In addition, for the good learners, we observed a sharp increase in the following response approximately 17 min after the beginning of training, which led to a difference in the cumulative number of rotations after 27 min (Figure S11; 27 min, good learners, 89.8 ± 11.3; poor learners, 54.6 ± 7.7; Tukey-Kramer test, $p < 0.05$). If predisposition had dominated memory for the imprinting stimulus, then these phenomena would not have been observed.

Brain asymmetry in birds, as in other vertebrate species, is well known, and the dominance of the left hemisphere in chick imprinting has been reported.[29–31] It has been suggested that NMDA receptors in the left hemisphere play an important part in imprinting.[32,33] Consistent

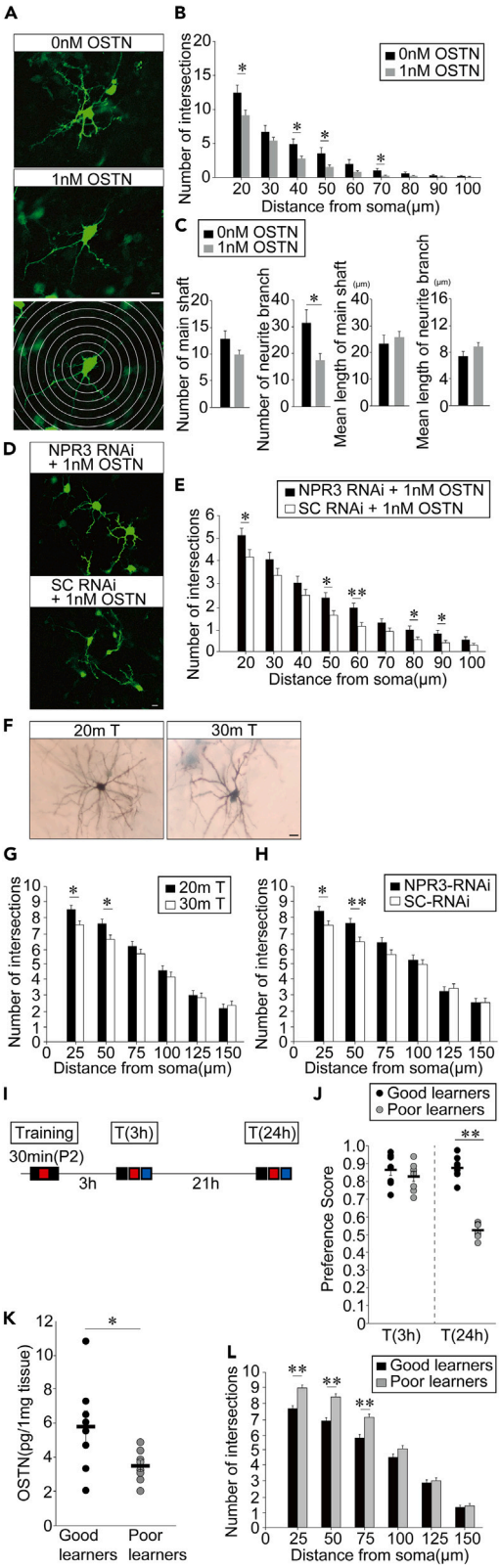

Figure 4. OSTN reduced the number of neurites in the embryonic brain, and long-term memory for the imprinting stimulus correlated with increased OSTN levels and reduced neurite branching in the left HA

(A) Micrographs of fluorescently labeled neurons in E8 brain slices. Circles are drawn every 10 μm from the center of the cell body. Scale bar, 10 μm.

(B) Sholl analysis showing numbers of dendritic intersections at each distance from the soma. The presence of 1 nM OSTN significantly reduced the number of neurites (0 nM OSTN, 22 cells from nine chicks, 1 nM OSTN, 28 cells from nine chicks).

(C) The effect of OSTN on the number and mean length of main shaft and neurite branch. The number of neurite branching was significantly reduced in the presence of 1 nM OSTN.

(D) Micrographs of fluorescently labeled neurons in E8 brain slices exposed to OSTN after NPR3-RNAi (upper) or scrambled RNAi (SC-RNAi) as a negative control (bottom). Scale bar, 20 μm.

(E) Sholl analysis showing numbers of dendritic intersections at each distance from the soma. Downregulation of NPR3 expression by RNAi rescued the inhibition of neurite outgrowth caused by the addition of OSTN (NPR3-RNAi, 51 cells from 14 chicks, SC-RNAi, 79 cells from 14 chicks).

(F) Representative micrographs of neurons with Golgi staining from 20m T to 30m T groups. Scale bar, 20 μm.

(G) Sholl analysis showing the number of dendritic crossovers every 25 μm from the soma. The number of neurites in 30m T was lower than that in 20m T (20m T, 120 cells from 12 chicks, 30m T, 120 cells from 12 chicks).

(H) Sholl analysis showing the number of dendritic intersections at each distance from the soma. Downregulation of NPR3 expression by RNAi rescued the inhibition of neurite outgrowth in 30m T group (NPR3-RNAi, 120 cells from 12 chicks, SC-RNAi, 120 cells from 12 chicks).

(I) Schedule of behavioral experiments.

(J) In 30m T group, chicks which showed high PS at T(3h) (PS > 0.70) were divided into two groups according to their T(24h) performance (good learners, PS > 0.70; poor leaners, PS < 0.60; $n = 8$ for each).

(K) The amount of OSTN peptide in the HA of chicks immediately after the evaluation at T(24h) was significantly higher in good learners than in poor learners.

(L) Sholl analysis showing the number of dendritic crossovers every 25 μm from the soma. The number of neurites in good learners was significantly lower than that in poor learners (good learners, 159 cells from 8 chicks; poor learners, 147 cells from 8 chicks). Data are represented as mean ± SEM. *, $p < 0.05$; **, $p < 0.01$. See also Figures S10and S11, and Tables S4–S8.

with these reports, we found that restricted ablation of the left hyperpallium densocellulare (HD) and the inhibition of the NMDA receptor, Trk, or A-type GABA receptor in the left dorsal telencephalon lead to impairment of imprinting.[2–4,34] Therefore, through *in vivo* studies and experiments using the chick telencephalon, we targeted or exclusively used the left telencephalon. The interhemispheric connections between HA and its role in imprinting should be the subject of further studies.

Loss-of-function mutations in NPR3 in mice indicate that the major function of NPR3 is to act as a clearance receptor for NP.[35–37] Some studies aimed at clarifying the action of OSTN in mammalian bones, and muscles have indicated that OSTN binding to NPR3 indirectly promotes the binding of CNP to NPR2, resulting in enhanced NPR2 action and bone and muscle growth.[12,20,38] However, in the HA of the chick telencephalon, OSTN and NPR3 were expressed (Figures 2B, 2C, and 2E), but not CNP3[9]; therefore, we focused on the effect of OSTN on NPR3. Injection of OSTN into HA resulted in the consolidation of acquired memory (Figures 3H–3J), and the knockdown of the NPR3 using shRNAi in HA inhibited the consolidation of memory (Figures 3K–3N). If OSTN enhanced the action of the CNP3-NPR2 or CNP3-NPR1 by reducing the binding of CNP3 to NPR3, the inhibitory effect of NPR3 shRNAi would not have been observed. From this evidence, we can conclude that OSTN-NPR3 signaling in HA neurons may be directly involved in the consolidation of memory for the imprinting stimulus rather than a secondary action of the NPR1 or NPR2.

A selective agonist of mammalian NPR3, c-ANF(C-ANP4-23) reduces adenylyl cyclase activity in membranes and intracellular concentrations of cAMP.[21] This phenomenon is inhibited by blocking the activity of Gi- or Go-proteins with pertussis toxin or by treating NPR3 with antisera raised against small peptide fragments of the NPR3 intracellular domain.[39,40] These reports indicate that NPR3 is not just a clearance receptor but also has intracellular signaling and physiological functions. Similarly, our results showed a decrease in the intracellular cAMP concentration in the NPR3-expressing HEK293 cells stimulated with OSTN (Figures 1F and 1G). An increase in intracellular cAMP concentration promotes neurite growth in various types of neurons. cAMP-dependent protein kinase A phosphorylates one of the small G proteins, Rho, which in turn inactivates Rho-ROCK signaling, resulting in neurite growth.[41–43] Therefore, when cellular cAMP levels are low, the active Rho-ROCK pathway may inhibit neurite growth. Studies on spatial or fear memory in rodents have revealed the involvement of the Rho-ROCK pathway in long-term memory.[44,45] Further studies are required to elucidate the precise mechanism by which OSTN suppresses neurite outgrowth.

Limitations of the study

With our injection and electroporation methods, we cannot target large areas in the HA. We found that OSTN injections or NPR3 RNAi were effective in the left ventral HA, near the border with the hyperpallium intercalatum/HD region. Therefore, our study suggests that a population of cells in the left ventral HA responded to OSTN. However, we cannot exclude the possibility that different cell populations in the HA respond to OSTN. Unfortunately, the detailed structure of the HA region, i.e., how and which population of neurons is distributed, remains unknown. Further detailed experiments, such as cell-specific knockdowns, will be necessary to specify which NPR3-positive cells in the HA are responsible for OSTN signaling.

RESOURCE AVAILABILITY

Lead contact

Further information and requests for resources and reagents should be directed to and will be fulfilled by the lead contact, Tomoharu Nakamori (tom-naka@kitasato-u.ac.jp).

Materials availability

All unique/stable reagents generated in this study are available from the lead contact without restriction.

Data and code availability

- The raw and processed data generated for this study have been deposited in Mendeley Data and are publicly available on the date of publication. The DOI is listed in the key resources table.
- This paper does not report the original code.
- Any additional information required to reanalyze the data reported in this paper is available from the lead contact upon request.

ACKNOWLEDGMENTS

This work was supported by JSPS KAKENHI (18K15350 and 21K12616) to T.N. and (19K06888) to H.O.-H. and a Kitasato University Research Grant for Young Researchers to T.N. Special thanks to Dr. Hara for teaching us the slice culture method using the developing brain, Kitasato University School of Medicine and School of Science for the experimental facility, and laboratory members for their help and discussions.

AUTHOR CONTRIBUTIONS

T.N., G.K., T.K., T.T., and H.O.-H. designed the research; T.N., I.K., U.I., A.M., K.F., and H.O.-H. performed the research; T.N., I.K., U.I., A.M., K.F., T.T., and H.O.-H. analyzed the data; and T.N. and H.O.-H. wrote the paper. All authors reviewed and edited the manuscript and approved the final version.

DECLARATION OF INTERESTS

The authors declare no competing interests.

DECLARATION OF GENERATIVE AI AND AI-ASSISTED TECHNOLOGIES IN THE WRITING PROCESS

During the preparation of this work, the author(s) used DeepL in order to improve the readability and language of the manuscript. After using this tool/service, the author(s) reviewed and edited the content as needed and take(s) full responsibility for the content of the publication.

STAR★METHODS

Detailed methods are provided in the online version of this paper and include the following:

SUPPLEMENTAL INFORMATION

Supplemental information can be found online at https://doi.org/10.1016/j.isci.2024.111195.

Received: September 28, 2023
Revised: February 17, 2024
Accepted: October 15, 2024
Published: October 18, 2024

REFERENCES

1. Lorenz, K.Z. (1937). The Companion in the Bird's World. Auk *54*, 245–273. https://doi.org/10.2307/4078077.
2. Nakamori, T., Sato, K., Atoji, Y., Kanamatsu, T., Tanaka, K., and Ohki-Hamazaki, H. (2010). Demonstration of a neural circuit critical for imprinting behavior in chicks. J. Neurosci. *30*, 4467–4480. https://doi.org/10.1523/JNEUROSCI.3532-09.2010.
3. Nakamori, T., Sato, K., Kinoshita, M., Kanamatsu, T., Sakagami, H., Tanaka, K., and Ohki-Hamazaki, H. (2015). Positive feedback of NR2B-containing NMDA receptor activity is the initial step toward visual imprinting: a model for juvenile learning. J. Neurochem. *132*, 110–123. https://doi.org/10.1111/jnc.12954.
4. Nakamori, T., Kato, T., Sakagami, H., Tanaka, K., and Ohki-Hamazaki, H. (2017). Regulation of visual Wulst cell responsiveness by imprinting causes stimulus-specific activation of rostral cells. Sci. Rep. *7*, 42927. https://doi.org/10.1038/srep42927.
5. Maekawa, F., Komine, O., Sato, K., Kanamatsu, T., Uchimura, M., Tanaka, K., and Ohki-Hamazaki, H. (2006). Imprinting modulates processing of visual information in the visual wulst of chicks. BMC Neurosci. *7*, 1–13. https://doi.org/10.1186/1471-2202-7-75.
6. Nakamori, T., Maekawa, F., Sato, K., Tanaka, K., and Ohki-Hamazaki, H. (2013). Neural basis of imprinting behavior in chicks. Dev. Growth Differ. *55*, 198–206. https://doi.org/10.1111/dgd.12028.
7. Bradley, P., and Horn, G. (1979). Neuronal plasticity in the chick brain: morphological effects of visual experience on neurones in hyperstriatum accessorium. Brain Res. *162*, 148–153. https://doi.org/10.1016/0006-8993(79)90764-9.
8. Horn, G., Bradley, P., and McCabe, B.J. (1985). Changes in the Structure of Synapses Associated with Learning. J. Neurosci. *5*, 3161–3168. https://doi.org/10.1523/JNEUROSCI.05-12-03161.1985.
9. Nakamori, T., Chiba, Y., Fujitani, K., Makita, A., Okubo, T., Hirai, K., Takamatsu, N., and Ohki-Hamazaki, H. (2019). Characteristic expressions of the natriuretic peptide family in the telencephalon of juvenile chick. Brain Res. *1708*, 116–125. https://doi.org/10.1016/J.BRAINRES.2018.12.007.
10. Thomas, G., Moffatt, P., Salois, P., Gaumond, M.H., Gingras, R., Godin, É., Miao, D., Goltzman, D., and Lanctôt, C. (2003). Osteocrin, a novel bone-specific secreted protein that modulates the osteoblast phenotype. J. Biol. Chem. *278*, 50563–50571. https://doi.org/10.1074/JBC.M307310200.
11. Nishizawa, H., Matsuda, M., Yamada, Y., Kawai, K., Suzuki, E., Makishima, M., Kitamura, T., and Shimomura, I. (2004). Musclin, a novel skeletal muscle-derived secretory factor. J. Biol. Chem. *279*, 19391–19395. https://doi.org/10.1074/JBC.C400066200.
12. Moffatt, P., Thomas, G., Sellin, K., Bessette, M.C., Lafrenière, F., Akhouayri, O., St-Arnaud, R., and Lanctôt, C. (2007). Osteocrin is a specific ligand of the natriuretic Peptide clearance receptor that modulates bone growth. J. Biol. Chem. *282*, 36454–36462. https://doi.org/10.1074/JBC.M708596200.
13. Kita, S., Nishizawa, H., Okuno, Y., Tanaka, M., Yasui, A., Matsuda, M., Yamada, Y., and Shimomura, I. (2009). Competitive binding of musclin to natriuretic peptide receptor 3 with atrial natriuretic peptide. J. Endocrinol. *201*, 287–295. https://doi.org/10.1677/JOE-08-0551.
14. Chinkers, M., Garbers, D.L., Chang, M.S., Lowe, D.G., Chin, H., Goeddel, D.V., and Schulz, S. (1989). A membrane form of guanylate cyclase is an atrial natriuretic peptide receptor. Nature *338*, 78–83. https://doi.org/10.1038/338078a0.

15. Chang, M.S., Lowe, D.G., Lewis, M., Hellmiss, R., Chen, E., and Goeddel, D.V. (1989). Differential activation by atrial and brain natriuretic peptides of two different receptor guanylate cyclases. Nature *341*, 68–72. https://doi.org/10.1038/341068a0.
16. Lowe, D.G., Chang, M.S., Hellmiss, R., Chen, E., Singh, S., Garbers, D.L., and Goeddel, D.V. (1989). Human atrial natriuretic peptide receptor defines a new paradigm for second messenger signal transduction. EMBO J. *8*, 1377–1384. https://doi.org/10.1002/j.1460-2075.1989.tb03518.x.
17. Schulz, S., Singh, S., Bellet, R.A., Singh, G., Tubb, D., Chin, H., and Garbers, D.L. (1989). The primary structure of a plasma membrane guanylate cyclase demonstrates diversity within this new receptor family. Cell *58*, 1155–1162. https://doi.org/10.1016/0092-8674(89)90513-8.
18. Fuller, F., Porter, J.G., Arfsten, A.E., Miller, J., Schilling, J.W., Scarborough, R.M., Lewicki, J.A., and Schenk, D.B. (1988). Atrial natriuretic peptide clearance receptor. Complete sequence and functional expression of cDNA clones. J. Biol. Chem. *263*, 9395–9401. https://doi.org/10.1016/S0021-9258(19)76554-5.
19. Maack, T., Suzuki, M., Almeida, F.A., Nussenzveig, D., Scarborough, R.M., McEnroe, G.A., and Lewicki, J.A. (1987). Physiological role of silent receptors of atrial natriuretic factor. Science *238*, 675–678. https://doi.org/10.1126/science.2823385.
20. Kanai, Y., Yasoda, A., Mori, K.P., Watanabe-Takano, H., Nagai-Okatani, C., Yamashita, Y., Hirota, K., Ueda, Y., Yamauchi, I., Kondo, E., et al. (2017). Circulating osteocrin stimulates bone growth by limiting C-type natriuretic peptide clearance. J. Clin. Invest. *127*, 4136–4147. https://doi.org/10.1172/JCI94912.
21. Anand-Srivastava, M.B., Sairam, M.R., and Cantin, M. (1990). Ring-deleted analogs of atrial natriuretic factor inhibit adenylate cyclase/cAMP system. Possible coupling of clearance atrial natriuretic factor receptors to adenylate cyclase/cAMP signal transduction system. J. Biol. Chem. *265*, 8566–8572. https://doi.org/10.1016/S0021-9258(19)38925-2.
22. Savoie, P., de Champlain, J., and Anand-Srivastava, M.B. (1995). C-type natriuretic peptide and brain natriuretic peptide inhibit adenylyl cyclase activity: interaction with ANF-R2/ANP-C receptors. FEBS Lett. *370*, 6–10. https://doi.org/10.1016/0014-5793(95)00780-d.
23. Murthy, K.S., and Makhlouf, G.M. (1999). Identification of the G protein-activating domain of the natriuretic peptide clearance receptor (NPR-C). J. Biol. Chem. *274*, 17587–17592. https://doi.org/10.1074/jbc.274.25.17587.
24. Ataman, B., Boulting, G.L., Harmin, D.A., Yang, M.G., Baker-Salisbury, M., Yap, E.L., Malik, A.N., Mei, K., Rubin, A.A., Spiegel, I., et al. (2016). Evolution of Osteocrin as an activity-regulated factor in the primate brain. Nature *539*, 242–247. https://doi.org/10.1038/NATURE20111.
25. Anand-Srivastava, M.B., Sehl, P.D., and Lowe, D.G. (1996). Cytoplasmic domain of natriuretic peptide receptor-C inhibits adenylyl cyclase: involvement of a pertussis toxin-sensitive G protein. J. Biol. Chem. *271*, 19324–19329. https://doi.org/10.1074/JBC.271.32.19324.
26. He, X.L., Chow, D.C., Martick, M.M., and Christopher Garcia, K. (2001). Allosteric activation of a spring-loaded natriuretic peptide receptor dimer by hormone. Science *293*, 1657–1662. https://doi.org/10.1126/SCIENCE.1062246.
27. Harada, K., Ito, M., Wang, X., Tanaka, M., Wongso, D., Konno, A., Hirai, H., Hirase, H., Tsuboi, T., and Kitaguchi, T. (2017). Red fluorescent protein-based cAMP indicator applicable to optogenetics and in vivo imaging. Sci. Rep. *7*, 7351. https://doi.org/10.1038/S41598-017-07820-6.
28. Puelles, L., Martinez-de-la-Torre, M., Paxinos, G., Watson, C., and Martínez, S. (2007). The Chick Brain in Stereotaxic Coordinates: An Atlas Featuring Neuromeric Subdivisions and Mammalian Homologies (Elsevier Science).
29. Gunturkun, O. (1997). Avian visual lateralization: a review. Neuroreport *8*. iii–xi.
30. Rogers, L.J. (2014). Asymmetry of brain and behavior in animals: Its development, function, and human relevance. Genesis *52*, 555–571. https://doi.org/10.1002/dvg.22741.
31. Gunturkun, O., and Ocklenburg, S. (2017). Ontogenesis of lateralization. Neuron *94*, 249–263. https://doi.org/10.1016/j.neuron.2017.02.045.
32. McCabe, B.J., and Horn, G. (1988). Learning and memory: regional changes in N-methyl-D-aspartate receptors in the chick brain after imprinting. Proc. Natl. Acad. Sci. USA *85*, 2849–2853. https://doi.org/10.1073/pnas.85.8.2849.
33. McCabe, B.J., Davey, J.E., and Horn, G. (1992). Impairment of learning by localized injection of an N-methyl-D-aspartate receptor antagonist into the hyperstriatum ventrale of the domestic chick. Behav. Neurosci. *106*, 947–953. https://doi.org/10.1037/0735-7044.106.6.947.
34. Suzuki, K., Maekawa, F., Suzuki, S., Nakamori, T., Sugiyama, H., Kanamatsu, T., Tanaka, K., and Ohki-Hamazaki, H. (2012). Elevated expression of brain-derived neurotrophic factor facilitates visual imprinting in chicks. J. Neurochem. *123*, 800–810. https://doi.org/10.1111/jnc.12039.
35. Potter, L.R., Abbey-Hosch, S., and Dickey, D.M. (2006). Natriuretic peptides, their receptors, and cyclic guanosine monophosphate-dependent signaling functions. Endocr. Rev. *27*, 47–72. https://doi.org/10.1210/ER.2005-0014.
36. Jaubert, J., Jaubert, F., Martin, N., Washburn, L.L., Lee, B.K., Eicher, E.M., and Guénet, J.L. (1999). Three new allelic mouse mutations that cause skeletal overgrowth involve the natriuretic peptide receptor C gene (Npr3). Proc. Natl. Acad. Sci. USA *96*, 10278–10283. https://doi.org/10.1073/PNAS.96.18.10278.
37. Matsukawa, N., Grzesik, W.J., Takahashi, N., Pandey, K.N., Pang, S., Yamauchi, M., and Smithies, O. (1999). The natriuretic peptide clearance receptor locally modulates the physiological effects of the natriuretic peptide system. Proc. Natl. Acad. Sci. USA *96*, 7403–7408. https://doi.org/10.1073/PNAS.96.13.7403.
38. Subbotina, E., Sierra, A., Zhu, Z., Gao, Z., Koganti, S.R.K., Reyes, S., Stepniak, E., Walsh, S.A., Acevedo, M.R., Perez-Terzic, C.M., et al. (2015). Musclin is an activity-stimulated myokine that enhances physical endurance. Proc. Natl. Acad. Sci. USA *112*, 16042–16047. https://doi.org/10.1073/PNAS.1514250112.
39. Pagano, M., and Anand-Srivastava, M.B. (2001). Cytoplasmic domain of natriuretic peptide receptor C constitutes Gi activator sequences that inhibit adenylyl cyclase activity. J. Biol. Chem. *276*, 22064–22070. https://doi.org/10.1074/JBC.M101587200.
40. Anand-Srivastava, M.B., Srivastava, A.K., and Cantin, M. (1987). Pertussis toxin attenuates atrial natriuretic factor-mediated inhibition of adenylate cyclase. Involvement of inhibitory guanine nucleotide regulatory protein. J. Biol. Chem. *262*, 4931–4934. https://doi.org/10.1016/S0021-9258(18)61132-9.
41. Jalink, K., Van Corven, E.J., Hengeveld, T., Morii, N., Narumiya, S., and Moolenaar, W.H. (1994). Inhibition of lysophosphatidate- and thrombin-induced neurite retraction and neuronal cell rounding by ADP ribosylation of the small GTP-binding protein Rho. J. Cell Biol. *126*, 801–810. https://doi.org/10.1083/JCB.126.3.801.
42. Threadgill, R., Bobb, K., and Ghosh, A. (1997). Regulation of dendritic growth and remodeling by Rho, Rac, and Cdc42. Neuron *19*, 625–634. https://doi.org/10.1016/S0896-6273(00)80376-1.
43. Dong, J.M., Leung, T., Manser, E., and Lim, L. (1998). cAMP-induced morphological changes are counteracted by the activated RhoA small GTPase and the Rho kinase ROKα. J. Biol. Chem. *273*, 22554–22562. https://doi.org/10.1074/JBC.273.35.22554.
44. Lamprecht, R., Farb, C.R., and Ledoux, J.E. (2002). Fear memory formation involves p190 RhoGAP and ROCK proteins through a GRB2-mediated complex. Neuron *36*, 727–738. https://doi.org/10.1016/s0896-6273(02)01047-4.
45. Dash, P.K., Orsi, S.A., Moody, M., and Moore, A.N. (2004). A role for hippocampal Rho-ROCK pathway in long-term spatial memory. Biochem. Biophys. Res. Commun. *322*, 893–898. https://doi.org/10.1016/J.BBRC.2004.08.004.
46. Maekawa, F., Nakamori, T., Uchimura, M., Fujiwara, K., Yada, T., Tsukahara, S., Kanamatsu, T., Tanaka, K., and Ohki-Hamazaki, H. (2007). Activation of cholecystokinin neurons in the dorsal pallium of the telencephalon is indispensable for the acquisition of chick imprinting behavior. J. Neurochem. *102*, 1645–1657. https://doi.org/10.1111/j.1471-4159.2007.04733.x.
47. Takahashi, T., Nakamura, F., and Strittmatter, S.M. (1997). Neuronal and non-neuronal collapsin-1 binding sites in developing chick are distinct from other semaphorin binding sites. J. Neurosci. *17*, 9183–9193. https://doi.org/10.1523/JNEUROSCI.17-23-09183.1997.
48. McCabe, B.J., Cipolla-Neto, J., Horn, G., and Bateson, P. (1982). Amnesic effects of bilateral lesions placed in the hyperstriatum ventrale of the chick after imprinting. Exp. Brain Res. *48*, 13–21. https://doi.org/10.1007/BF00239568.
49. Hara, Y., Fukaya, M., Hayashi, K., Kawauchi, T., Nakajima, K., and Sakagami, H. (2016). ADP ribosylation factor 6 regulates neuronal migration in the developing cerebral cortex through FIP3/Arfophilin-1-dependent endosomal trafficking of N-cadherin. eNeuro *3*, ENEURO.0148-16.2016. https://doi.org/10.1523/ENEURO.0148-16.2016.

STAR★METHODS

KEY RESOURCES TABLE

REAGENT or RESOURCE	SOURCE	IDENTIFIER
Antibodies		
Anti-DIG antibody	Roche Applied Science	Cat# 11093274910; RRID: AB_514497
Anti-AP antibody	GenHunter Corporation	Cat# Q301
Anti-HA antibody	Roche Applied Science	Cat# 11583816001; RRID: AB_514505
Anti-GFP antibody	Thermo Fisher Scientific	Cat# A11122; RRID: AB_221569
Anti-β-actin antibody	Santa Cruz Biotechnology	Cat# sc47778; RRID: AB_626632
Anti-rabbit IgG antibody	Cell Signaling Technology	Cat# 7074S; RRID: AB_2099233
Anti-mouse IgG antibody	Cell Signaling Technology	Cat# 7076S; RRID: AB_330924
Chemicals, peptides, and recombinant proteins		
RNeasy Plus Micro Kit	QIAGEN	Cat# 74034
PrimeScript II 1st Strand cDNA Synthesis Kit	Takara Bio Inc.	Cat# 6210A
KOD FX *Neo*	TOYOBO	Cat# KFX201
SsoAdvanced Universal SYBR Green Supermix	Bio-Rad Laboratories	Cat# 1725271
Tissue-Tek O.T.C. Compound	Sakura Finetek	Cat# 831824
RNA labeling kit	Roche Applied Science	Cat# 11277073910
T3 RNA Polymerase	Roche Applied Science	Cat# 11031171001
T7 RNA Polymerase	Roche Applied Science	Cat# 10881775001
Blocking reagent	Roche Applied Science	Cat# 11112589001
NBT/BCIP	Roche Applied Science	Cat# 11681451001
Hemo-De	FALMA	Cat# CS1001
PARAmount-N	FALMA	Cat# 308401
Platinum SuperFi DNA polymerase	Thermo Fisher Scientific	Cat# 12351010
DMEM	Wako	Cat# 04129775
Fetal bovine serum	Biowest	Cat# S1810
Penicillin-streptomycin	Sigma-Aldrich	Cat# 4333
CAPHOS	Sigma-Aldrich	Cat# 2331408
Lipofectamine3000	Invitrogen	Cat# L3000008
G418	Nacalai Tesque	Cat# 09380-86
Isobutylmethylxanthine	Sigma-Aldrich	Cat# 28822584
AP-OSTN	This paper	Cat# N/A
chOSTN(24) peptide	PH Japan	Cat# N/A
Neurobasal Medium	Thermo Fisher Scientific	Cat# 21103049
B27	Thermo Fisher Scientific	Cat# 17504044
BLOCK-itTM Pol II miR Expression Kit with EmGFP	Thermo Fisher Scientific	Cat# K493600
FD Rapid GolgiStain Kit	FD NeuroTechnologies	Cat# PK401
Phosphatase inhibitor cocktails	Sigma-Aldrich	Cat# PPC1010
DNase I	Roche Applied Science	Cat# 4716728001
Transfer membranes	Merck Millipore	Cat# IPVH07850
ImmunoBlock Solution	KAC	Cat# CTKN001
Can Get Signal Solution 1	TOYOBO	Cat# NKB201
Can Get Signal Solution 2	TOYOBO	Cat# NKB301
Pierce Western Blotting Substrate	Thermo Fisher Scientific	Cat# 10005943

(*Continued on next page*)

Continued

REAGENT or RESOURCE	SOURCE	IDENTIFIER
Experimental models: Cell lines		
Human: HEK293 cells	Riken BRC	RBRC-RCB1637
Human: HEK293T cells	Riken BRC	RBRC-RCB2202
Oligonucleotides		
Primers, and designed oligonucleotides for shRNAi	This paper	See Table S9
Recombinant DNA		
pcDNA3-chNPR3-HA	This paper	Cat# N/A
pEGFP-N2	Clontech	Cat# 6081-1
pcDNA3-EGFP	This paper	Cat# N/A
Software and algorithms		
BellCurve for Excel	Social Survey Research Information Co., Ltd.	RRID: SCR_017294
VSG	Cambridge Research Systems Ltd.	Cat# N/A
SOFTmax Pro 4.0	Molecular Devices	RRID: SCR_014240
Other		
Syringe	Hamilton Company	Cat# 4015-12001
Histological Slides	Matsunami	Cat# SMAS-01
6-well plate	Thermo Fisher Scientific	Cat# 140675
35 mm dish with a glass base	Corning	Cat# 430165
35 mm dish	Iwaki	Cat# 3000-035
Insert membrane	Millipore	Cat# PICM0RG50
Raw data	This paper	Mendeley Data: https://data.mendeley.com/preview/2d4xsph6jn?a=260cab86-47b9-4290-8509-9a57b24591a5

EXPERIMENTAL MODEL AND STUDY PARTICIPANT DETAILS

Animals

Fertilized eggs from White Leghorn chickens of the Julialite strain (*Gallus gallus domesticus*) were obtained from local suppliers (Nihon Layer, Gifu, Japan) and allowed to develop in an incubator at 37.7°C with moderate moisture and quasi-constant darkness. After hatching, chicks of both sexes were maintained in groups in the same incubator. This study was conducted in accordance with the Regulations for the Care and Use of Laboratory Animals of Kitasato University. Experimental protocols described in this paper were approved by the Institutional Animal Care and Use Committee of Kitasato University.

METHOD DETAILS

Reverse-transcription PCR

Sagittal sections with a thickness of 2 mm were produced by cutting 1 mm and 3 mm laterally from the midline of the left telencephalon of chicks at 1 or 7 days after hatching, and the rostral region of the HA (approximately 8 mm^3) was dissected from these sections (Figure 2A inset). Additionally, the dorsal-caudal region of the telencephalon (approximately 8 mm^3) was excised from the embryonic stage of the chicks. Total RNA was extracted using the RNeasy Plus Micro Kit (QIAGEN, Hilden, Germany) and cDNA was synthesized using the PrimeScript II 1st Strand cDNA Synthesis Kit with oligo dT primers (Takara Bio Inc., Shiga, Japan). RT-PCR was performed with the primers listed in Table S9 using KOD FX *Neo* (TOYOBO, Osaka, Japan). The reaction program included 30 or 40 cycles of 30 s at 98°C, 10 s at 62°C, and 10 s at 68°C.

In situ hybridization

In situ hybridization was performed using free-floating sections according to procedures previously described.[2,34,46] Whole brains were fixed with 4% paraformaldehyde for about 16 h at 4°C, cryoprotected by immersing in 30% sucrose for 48 h, embedded in the Tissue-Tek O.T.C. Compound (Sakura Finetek Japan, Tokyo, Japan), and frozen in powdered dry ice. Using a cryostat (CM1520, Leica Microsystems, Wetzlar, Germany), sagittal sections (50-μm thickness) were prepared. The sections were stored at −80°C in 25 mM phosphate buffer (PB) containing 50% glycerol, 8.6% sucrose, 0.4% sodium chloride (NaCl) and 3.2 mM magnesium chloride ($MgCl_2$).

Chicken OSTN (XM_025153364) and NPR3 (XM_046936337) gene fragments with the sequences of T3 (5′-ATTAACCCTCACTAAAGGGA-3′) or T7 promoter (5′-TAATACGACTCACTATAGGG-3′) were amplified from chick brain cDNAs using the primers described in Table S9. Gene-specific sense and antisense digoxigenin (DIG)-labeled cRNA probes were generated using the Roche RNA labeling kit (Roche Applied Science, IN, USA).

For floating sections, *in situ* hybridization was performed as follows: After fixation with 4% paraformaldehyde in 50 mM PB, the sections were washed twice with 10 mM PB, treated with proteinase K (1 μg/mL) in Tris-ethylenediaminetetraacetic acid (EDTA) buffer (pH 8.0) at room temperature (25°C) for 10 min, and acetylated with 0.25% acetic anhydride in 100 mM triethanolamine for 10 min. Hybridization was performed at 60°C for 14–16 h in a solution containing 50% formamide, 2% blocking reagent (Roche Applied Science), 5× saline sodium citrate (5× SSC; 750 mM NaCl, 75 mM trisodium citrate dehydrate), 0.1% N-lauroylsarcosine, 0.1% sodium lauryl sulfate, and DIG-labeled cRNA probe. The sections were washed sequentially at 60°C with a solution containing 50% formamide and 2× SSC for 30 min, 2× SSC for 30 min, and 0.2× SSC for 30 min, followed by treatment with DIG-1 buffer (100 mM Tris-HCl pH 7.5, 150 mM NaCl, 0.1% Tween 20). The sections were incubated in blocking buffer (5% bovine serum albumin [BSA] in DIG-1 buffer) for 2 h at room temperature. After blocking, the sections were transferred to alkaline phosphatase-conjugated anti-DIG antibody (1:2000 dilution; Roche Applied Science) in blocking buffer and incubated overnight at 4°C. After incubation, the sections were washed three times with DIG-1 buffer for 15 min, rinsed with DIG-3 buffer (in mM: 100 Tris–HCl pH 9.5, 100 NaCl, 50 $MgCl_2$), and incubated in nitro blue tetrazolium chloride plus 5-bromo-4-chloro-3-indolyl phosphate (NBT/BCIP; 1:50 in DIG-3 buffer; Roche Applied Science) for 2–10 h at 25°C. Sections were washed with Tris-EDTA buffer (pH 8.0) and mounted on slides in 50 mM PB containing 20% ethanol. After drying, samples were dehydrated in ethanol, immersed in Hemo-De (FALMA, Tokyo, Japan), and mounted in PARAmount-N (FALMA).

Real-time PCR

To examine the expression level of OSTN and NPR3, sagittal sections with a thickness of 1 mm were produced by cutting 1 mm and 2 mm laterally from the midline of the left telencephalon of chicks, and the rostral region of the HA (approximately 1 mm^3) was dissected from these sections (Figure 3B inset). Total RNA was extracted and cDNA was synthesized as above. Then, real-time PCR was performed using gene-specific primers (Table S9) and SsoAdvanced Universal SYBR Green Supermix (Bio-Rad Laboratories, Hercules, CA, USA). The fluorescence signal was detected using CFX96 Touch Real-Time PCR Detection System (Bio-Rad Laboratories). The reaction program comprised 40 cycles of 10 s at 95°C and 10 s at 55°C. The expression level of each gene was calculated relative to that of chicken glucuronidase-beta gene (GUSB, NM_001039316.2). Cloning of chNPR3v1-2.

Complementary DNA prepared from P1 and P7 chick VW was used as a template to obtain a fragment of the predicted chNPR3v1-2 gene corresponding to the entire coding region by PCR with Platinum SuperFi DNA polymerase (Thermo Fisher Scientific, MA, USA) using forward (EcoRI-NPR3-Fw) and reverse (XhoI-NPR3-1-2-Rv) primers (Table S9). Amplified fragment was cloned into pBluescriptIIsk(−) and the sequence was verified.

Preparation of stable cell lines

The HA-tagged chNPR3 fragment containing the entire coding region was obtained by PCR with primers EcoRI-NPR3-Fw and XhoI-HA-NPR3 (2)-Rv (Table S9) using cloned chNPR3v1-2 (#15) as a template. The amplified products were then subcloned into pcDNA3 and the sequence was verified. The pcDNA3/chNPR3v1-2-HA plasmid encoding the correct amino acid sequence (#13) was used for transfection. As a control, the EGFP fragment was excised from pEGFP-N2 (Clontech, CA, USA) using EcoRI and NotI and cloned into pcDNA3 to yield pcDNA3/EGFP. HEK293 cells maintained in Dulbecco's modified Eagle's medium (DMEM; Sigma-Aldrich, MO, USA) supplemented with 10% fetal bovine serum (Biowest, Nuaille, France), 100 U/mL penicillin and 100 μg/mL streptomycin (Sigma-Aldrich) were seeded in a 6-well plate (6×10^5 cells/well). Twenty-four hours later, cells were transfected either with pcDNA3/chNPR3v1-2-HA vector, or pcDNA3/EGFP vector (5 μg/well) by calcium phosphate methods (CAPHOS, Sigma-Aldrich). One day after transfection, cells were plated in 90 mm plates. After 3-week selection with 500 μg/mL G418 (Nakalai Tesque, Kyoto, Japan), colonies were picked up and cells were frozen. Proteins extracted from the chNPR3v1-2-HA expressing clones were subjected to western blot analysis, and the presence of chNPR3v1-2-HA was verified using an anti-HA antibody. EGFP expression was verified by observing the fluorescence under a microscope. Clones that highly expressed EGFP or HA were selected as the stable cell lines.

Preparation of chOSTN-alkaline phosphatase fusion protein (AP-chOSTN)

A fragment of chOSTN containing the coding region was amplified by PCR with Platinum SuperFi DNA polymerase (Thermo Fisher Scientific, MA, USA) using forward (XhoI-chOSTN(82)-Fw) and reverse (XbaI-chOSTN(399)-Rv) primers (Table S9). Complementary DNA prepared from P7 chick VW was used as template. The amplified fragment was cloned into pAPtag-5 (GenHunter, TN, USA), and the sequence of the resulting plasmid pAPtag-5/chOSTN was verified.[11] HEK293T cells were seeded in a 6-well plate for transfection as HEK293 cells described above. Transfection was performed with the pAPtag-5/chOSTN vector or pAPtag vector without an insert (2.5 μg/well) using Lipofectamine3000 (Invitrogen, MA, USA). Six days after the transfection, medium was collected and stored at 4°C. The collected medium was subjected to western blot analysis and the presence of AP or AP-OSTN protein was verified using an anti-AP antibody (Figure S1).

Staining of AP-OSTN for cultured cells

Cells were pre-washed in phosphate-buffered saline (PBS) and equilibrated with HBH (Hank's balanced salt buffer with 0.5 mg/mL BSA and HEPES [20 mM], pH 7.0) for 5 min. After treatment for 15 min with DMEM containing 10% fetal bovine serum and 100 IU/mL penicillin-streptomycin (DMEM/FBS), cells were incubated with collected AP-OSTN medium or collected AP-OSTN medium containing 1μM OSTN peptide for 2 h. Cells were washed with ice-cold HBH 6 times for 3 min each, and fixed with 4% PFA in HBH for 15 min. Cells were washed twice with HH buffer (Hank's balanced salt buffer and 20 mM HEPES, pH 7.0) for 3 min each and incubated in HH at 65°C for 120 min to inactivate heat-sensitive endogenous alkaline phosphatases. Then, cells were incubated in NBT/BCIP (1:50 in DIG-3 buffer) for 24 h at 4°C, and washed with Tris-EDTA buffer (pH 8.0).

Staining of AP-chOSTN for tissue sections

Staining of AP-OSTN protein in tissue sections was performed with reference to Takahashi et al. (1997).[47] Brains of P1 chicks were frozen on dry ice, and 50-μm-thick sections were cut on a cryostat and mounted onto slides. Sections were fixed with 100% methanol at −80°C for 10 min. The fixed sections were rehydrated in PBS, equilibrated with HBH for 5 min, and treated with HBH containing 20% fetal bovine serum for 1 h. The sections were then incubated for 2 h with AP-OSTN fusion protein or AP protein diluted in HBH containing 20% fetal bovine serum. Sections were washed once with HBH for 5 min, with Tris-buffered saline (20 mM Tris-HCl and 135 mM NaCl, pH 7.5) three times for 5 min each, with PBS for 5 min, and fixed with 4% formaldehyde in PBS for 15 min. The fixed sections were incubated in PBS at 65°C for 50 min to inactivate heat-sensitive endogenous alkaline phosphatases. Then, they were incubated in NBT/BCIP (1:50 in DIG-3 buffer) for 4 h at 25°C. The sections were then washed with Tris-EDTA buffer (pH 8.0). After drying, the samples were dehydrated in ethanol, immersed in Hemo-De, and mounted in PARAmount-N.

Detection of the effect of chOSTN on cyclic AMP concentration in NPR3v1-2 expressing cells

HEK293 cells stably expressing the NPR3v1-2 or non-transfected HEK293 cells were seeded in 35 mm dish with a glass base (Corning, AZ, USA) at a density of 6×10^5 cells/dish. Twenty-four hours later, cells were transfected with Pink Flamindo expression vector[27] (2.5 μg/dish) by using Lipofectamine3000 (Invitrogen). Two days later, the cells were washed twice with 2 mL DMEM and incubated in 2 mL DMEM before imaging. Fluorescence images were acquired using a confocal laser microscope (LSM710; Carl Zeiss, Oberkochen, Germany). Images were acquired every 2 min for 40 min using 565 nm excitation and 590 nm emission filters. Ten minutes after the start of imaging, OSTN was added to DMEM at a final concentration of 0.1 nM, and after 30 min from the start OSTN was washed away with fresh DMEM. Data analysis of the acquired images was performed using the NIH-Image software, and the fluorescence intensity of the cells was quantified. After subtracting the background, the fluorescence intensity of each cell in the first image was used as baseline intensity. This value was normalized to 100%. Fluorescence images of the NPR3v1-2-expressing and non-transfected HEK293 cells were obtained on six plates, and the relative fluorescence intensity of 20 cells per plate was calculated.

Imprinting device

We used a visual imprinting device, as described previously[2–5,46] with slight modifications. Two running wheels connected to a custom-made computer system were used to record the movements of the chicks toward or away from the display (Muromachi Kikai, Tokyo, Japan). Two wheels (diameter 40 cm) were placed side by side in the center of a vinyl box (D 50 cm × W 70 cm × H 50 cm). Because one of the sidewalls of each wheel facing the other wheel was made of a transparent acrylic board, an opaque plastic board was placed between the wheels. A 21.3-inch (Flex Scan S2133-H; EIZO, Ishikawa, Japan) liquid crystal screen was placed outside the vinyl box 20 cm from the end of the wheel, and an image was displayed on the screen with a black background. The vinyl box had a transparent roof, and all walls were black, except for the wall through which the screen could be seen. The apparatus was illuminated with an LED lamp and the inside of the wheels was 280 lx. The images were generated using a visual stimulus generator system (VSG; Cambridge Research Systems Ltd., Kent, UK). A square had 8.6 cm-long sides (12° visual field of the chick at the bottom of the wheel) and bounced left and right horizontally on the screen at a rate of 7.3 cm/s (10.4°/s). The RGB values for red and blue were 255, 0, 0, and 0, 0, 255, respectively.

Presentation of visual stimulus and evaluation of visual imprinting

The chicks were placed individually on the running wheel. The chicks were exposed to a moving red square on the screen for 20 or 30 min, and then returned to the dark incubator. Three or 24 h after training, the chicks were placed in the imprinting apparatus again. After a 5-min adaptation period (black screen, no presentation of the image), the red square (training image) and blue square (new image) were presented sequentially every 5 min on the screen. The direction and number of wheel rotations were recorded. We calculated the preference score (PS)[2,48] using the following formula as an index of the success of visual imprinting: PS = SUM (training image)/{SUM (training image) + SUM (new image)}, where SUM (training image) is the number of wheel rotations toward the screen during the presentation of the training stimulus, and SUM (new image) is the number of wheel rotations toward the screen during the presentation of the new image. Chicks that rotated the wheel by < 22.5 rotations during the 15-min evaluation period were excluded from the analysis.[34]

Peptide

ChOSTN (24) was custom-made and purchased from PH Japan Co., Ltd. (Hiroshima, Japan). The amino acid sequence of the chOSTN(24) peptide is ELPKRRFGVPLDRIGVSRLGNTKG.

Microinjection into the left HA region

Microinjections were performed as previously described.[2,4] ChOSTN(24) solution (1 nM chOSTN, 0.1% Evans blue dye, in 10 mM PBS, 2 μL) was injected with a syringe (701RN 10 μL SYR; Hamilton Company, Reno, NV, USA) into the left HA of anesthetized chicks. The chick head was held in a horizontal position, and the injection was positioned 8 mm rostral from the bregma, 1 mm left from the midline and 1-mm depth from the skull surface. A tube was attached to the outside of the needle to control the needle tip depth. The solution was injected slowly (approximately 2 μL/min), and approximately 1 min after the injection was complete, the needle was withdrawn.

Knockdown vector of NPR3

For NPR3 knockdown experiments, we used the BLOCK-it Pol II miR Expression Kit with EmGFP (Invitrogen). The target sequence selected for NPR3 knockdown was 5′-ATGAGCAGCCAACATGATGTT-3′ and two complementary oligonucleotides (the top and bottom strands) were designed according to the manufacturer's indication, except for the sequence of the hairpin loop, which was 5′-AACATCATTGGCTGCT CAT-3′ (NPR3-RNAi). Oligonucleotides were annealed and ligated into the vector. For a control plasmid vector, a scrambled mismatched sequence, 5′-AATAGAGACTGTCGATGTACC-3′ was used (SC-RNAi).

NPR3-RNAi *in vivo*

A freehand injection into the left HA (10 mm rostral from the bregma, 1 mm left from the midline and 1-mm depth from the skull surface) was administered to anesthetized P1 chicks. Either NPR3-RNAi vector (2 μM, 2 μL) or SC-RNAi vector (2 μM, 2 μL), containing 0.1% Evans blue dye was injected with the syringe as described in "Microinjection into the left HA region". After 10 min, the chicks were held by hand, a platinum plate tweezer electrode (CUY 650 P3; Protech, Monroe, NC, USA) was placed on the head covered with glycerol, and five square pulses (100 V, 50 ms) at 1 Hz were applied using an ElectroSquarePorator (ECM830; Harvard Apparatus, Holliston, MA, USA).

Slice culture

Brains from E8 chicks were embedded in 3% low melting temperature agarose gel and sliced into 200-μm-thick coronal sections in ice-cold PBS using a microslicer (DTK-3000W; Dousaka, Kyoto, Japan). The slices containing HA region were placed on an insert membrane (Millipore) and maintained in dishes (Iwaki) filled with Neurobasal Medium (Thermo Fisher Scientific) containing 1% B27 (Invitrogen, San Diego, CA), and incubated in a CO_2 incubator (5% CO_2 at 37°C).[49]

Electroporation on slice culture

Each plasmid was mixed to 2 μg/μL solution in distilled water containing 50% glycerol. Two microliters of the mixed solution were placed on the HA region of the prepared slices, and three square pulses (10 V, 50 ms) at 1 Hz were applied using the ElectroSquarePorator with a platinum plate electrode and a needle-shaped electrode made of platinum wire (diameter, 0.25 mm; PT-351285, Nilaco, Tokyo, Japan).

Fluorescent image quantification of cultured cells

Individual EGFP-positive neurons used for analyses were selected and imaged using a confocal laser microscope (LSM710) with a 20× objective in a blinded manner. The number of dendritic intersections at 10-μm intervals from the center of the cell body was counted. The number and mean length of the main shaft and neurite branches were measured.

Golgi staining

The Golgi silver impregnation was done according to the protocol of a commercially available kit (FD Rapid GolgiStain Kit, FD NeuroTechnologies, MD, USA). Brain sagittal sections at 200 μm thickness were obtained with a microslicer (DTK-3000W), mounted on the slide glass, and imaged. Golgi-stained cells, morphologically identified as neurons, were photographed in a blinded manner using a microscope (CX41, Olympus, Tokyo, Japan) and a Nikon 1 J1 camera (Nikon, Tokyo, Japan) with an NY-1S adaptor (Micronet, Saitama, Japan). Five to ten neurons in the HA were imaged from at least three slices per chick (Figures 4G and 4H, $n = 12$/group; Figure 4L, $n = 8$/group). The number of dendritic intersections at 25-μm intervals from the center of the cell body was counted.

Protein extraction from HEK293 cells for western blotting

The cells were homogenized in ice-cold cell lysis buffer (150 mM NaCl, 1 mM EDTA, 100 mM sodium fluoride [NaF], 0.1 mM phenylarsine oxide, 10 mM pyrophosphoric acid, and 20 mM Tris-HCl; pH 7.4, including 1% Triton X-) supplemented with 1% protease and 1% phosphatase inhibitor cocktails (Sigma-Aldrich), incubated on ice for 20 min, and sonicated using an ultrasonic disruptor (UD-200; TOMY, Tokyo, Japan). After reacting with 4 units of DNase I (Roche Applied Science) per 1 μL of the protein extract at 37°C for 30 min, EDTA was added to a concentration of 0.02 M and heated at 80°C for 2 min. The suspension was centrifuged at 16,000 × g for 5 min at 4°C, and the supernatant was

collected and used as the total protein extract. The content of the extracted protein was determined by Bio-Rad protein assay (Bio-Rad Laboratories) with BSA as a standard using a microplate reader (VERSAmax; Molecular Devices) with a SOFTmax Pro 4.0 software (Molecular Devices).

Western blot analysis

Protein samples (5 μg per lane) were separated by 10% sodium dodecyl sulfate-polyacrylamide gel electrophoresis under reducing conditions, and the proteins in the gel were electroblotted onto nitrocellulose membranes (Merck Millipore, NJ, USA). The membranes were soaked in ImmunoBlock Solution (DS pharma biomedical, Osaka, Japan) and incubated with primary antibody, that was anti-HA (12CA5, Roche Applied Science), anti-GFP (A11122, Thermo Fisher Scientific) or anti-β-actin (sc-47778, Santa Cruz Biotechnology, TX, USA), (1:1000) in Can Get Signal Solution 1 (TOYOBO) at 4°C overnight. The blots were reacted with a secondary antibody, which was anti-rabbit IgG (7074S, Cell Signaling Technology) or anti-mouse IgG (7076S, Cell Signaling Technology) conjugated with horseradish peroxidase (1:1000) in Can Get Signal Solution 2 (TOYOBO) for 2 h at room temperature (25°C). Signals were visualized using Pierce Western Blotting Substrate (Thermo Fisher Scientific). Images were acquired using a Luminograph I detector (ATTA).

QUANTIFICATION AND STATISTICAL ANALYSIS

Statistical analysis was performed using a statistical software (BellCurve for Excel; Social Survey Research Information Co., Ltd., Tokyo, Japan). All data in this study are expressed as means ± SEM. The numbers of animals or samples used are indicated in the figure legends. We used one-way ANOVA, followed by the Tukey-Kramer test to compare the values between conditions (Figures 1G and 1H), and Dunnett's test to compare with the control value (Figure 3C). two-way ANOVA, followed by the Tukey-Kramer test, was used to compare the groups for two different categorical variables (Figure S11). The differences between the two experimental groups were analyzed using Student's *t*-test (Figures 3B, 3F, 3G, 3M, 3N, 4B, 4C, 4E, 4G, 4H, 4J, 4K, and 4L, S6, S9 and S10). To examine whether the PS values differed significantly from chance (0.5), a one-sample *t*-test was used (Figures 3E, 3J, and 3L). The difference in PS between the T(3h) and T(24h) was examined using a paired *t*-test (Figures 3E and 3L). Differences were considered statistically significant at $p < 0.05$ (* and #, $p < 0.05$; ** and ##, $p < 0.01$). The exact *p*-values are shown in the results (Figures 3B, 3E, 3F, 3G, 3J, 3L, 3M, 3N, 4C, 4J, 4K, S6, S9, S10, and S11) or Tables S1–S8 (Figures 1G, 1H, 3C, 4B, 4E, 4G, 4H, and 4L).